FeS Colloids – Formation and Mobilization Pathways in Natural Waters

Journal:	*Environmental Science: Nano*
Manuscript ID	EN-ART-12-2019-001427.R1
Article Type:	Paper

ENVIRONMENTAL SIGNIFICANCE STATEMENT

Colloids mediate the mobility of nutrients, metals and radionuclides in sediments that experience strong wet-dry cycling and thus impact groundwater quality. Sulfidation of Fe(III-hydroxide nanoparticles has been proposed to generate sulfidic colloids. However, their nature and the parameters controlling their formation are not well understood. Such information would improve understanding of their impact on water quality. We found that in fresh groundwater systems poor in sulfate (*i.e.* low sulfidation; lakes, floodplains, peatlands), sulfidation of ferrihydrite generates FeS colloids that remain suspended over long time periods, thus mobilizing a substantial fraction of the Fe and sulfide budgets. These results provide a conceptual model for predicting under what conditions FeS colloids form and enhance or inhibit the mobility of contaminants and nutrients associated with them.

FeS Colloids – Formation and Mobilization Pathways in Natural Waters

Vincent Noël[a,*], Naresh Kumar[b,c,d], Kristin Boye[a], Lilia Barragan[a], Juan Lezama-Pacheco[e], Rosalie Chu[f], Nikola Tolic[f], Gordon E. Brown Jr.[a,b,d], John R. Bargar[a]

[a] *Stanford Synchrotron Radiation Lightsource, SLAC National Accelerator Laboratory, 2575Sand Hill Road, Menlo Park, CA 94025, USA*

[b] *Department of Geological Sciences, School of Earth, Energy & Environmental Sciences, Stanford University, Stanford, CA 94305-2115, USA*

[c] *Department of Environmental Geosciences, Centre for Microbiology and Environmental Systems Science, University of Vienna, 1090 Vienna, AUSTRIA*

[d] *Center for Environmental Implications of NanoTechnology (CEINT), Duke University, P.O. Box 90287, Durham, NC 27708-0287, USA*

[e] *Department of Earth System Science, Stanford University, Stanford, CA 94305, USA*

[f] *Environmental Molecular Sciences Laboratory, Pacific Northwest National Laboratory, Richland, WA 99354, USA*

to be submitted to

Environmental Science Nano

*Corresponding author: Vincent Noël; e-mail: noel@slac.stanford.edu

ABSTRACT

We have used synchrotron-based X-ray absorption spectroscopy (structure of Fe-S clusters), transmission electron microscopy (solid-phase crystallinity), Fourier-transform ion-cyclotron-resonance mass spectrometry (identity and composition of natural organic carbon compounds), inductively coupled plasma optical emission spectrometry (total aqueous Fe), and the revised ferrozine method (aqueous Fe(II) and Fe(III) concentrations) to determine the stability and nature of colloids generated by sulfidation of ferrihydrite nanoparticles in the absence and presence of organic compounds. We observed that reductive dissolution of ferrihydrite by aqueous sulfide generates nm-scale FeS clusters. Their subsequent aggregation, which promotes settling of FeS aggregates into the solid fraction, was directly correlated with sulfide/Fe ratio. At sulfide/Fe ratios ≤0.5, FeS clusters and larger colloids remained in suspension for at least 14 days (and up to several months). At sulfide/Fe ratios >0.5, sulfidation reaction rates were rapid and FeS cluster aggregation was accelerated. Moreover, the presence of organic compounds increased the time of suspension of FeS colloids, whereas increased ionic strength inhibited the generation of FeS colloids. We present a general conceptual model to predict when and where FeS colloids can form and enhance or inhibit the mobility of contaminants and nutrients associated with them. Our study indicates that in low-salinity fresh groundwater systems poor in sulfate (*i.e.* low sulfidation; lakes, floodplains, peatlands *etc.*), the ferrihydrite sulfidation reaction generates aqueous FeS clusters and larger colloids that remain suspended over long time periods, thus mobilizing a substantial fraction of the total aqueous Fe and S.

Keywords: Groundwater quality; Sediment-water interaction; Colloids/nanoparticles; Dissolved Organic Carbon; sulfidation reaction

ABBREVIATIONS

DOE, Department of Energy; SSRL, Stanford Synchrotron Radiation Lightsource; ICP-OES, Inductively Coupled Plasma Optical Emission Spectrometry; FT-ICR-MS, Fourier-Transform Ion Cyclotron Resonance Mass Spectrometry; XAS, X-ray Absorption Spectroscopy; XANES, X-ray Absorption Near Edge Structure; EXAFS, X-ray Absorption Fine Structure; LC-LS, Linear Combination-Least Squares; TEM, Transmission Electron Microscopy; Fh, Ferrihydrite; OM, Organic Matter; PAA, Polyacrylic Acid; NOC, Natural Organic Carbon.

1. INTRODUCTION

Colloid-facilitated transport enhances the mobility of nutrients[1-3] and contaminants, such as heavy metals,[4-7] radionuclides,[8-13] pesticides,[14-17] and animal hormones and veterinary antibiotics,[18-20] mediating groundwater quality and nutrient and organic carbon transport.[21-23] Recurring seasonal wetting and drying of floodplain sediments drives redox processes at sediment-water interfaces.[6,24-28] Under sulfate-reducing conditions, metal sulfide precipitation has been proposed to generate colloidal particles[6,29-32] as well as smaller aqueous complexes, which we refer to as clusters in this paper, based on the findings of Luther and Rickard,[33] which can aggregate to form larger colloids.[35] Laboratory studies of the stability of aqueous metal (poly)sulfide and polynuclear clusters suggest that such dissolved clusters can sorb and transport contaminants in sulfidic environments.[33] Furthermore, aqueous metal sulfide clusters are remarkably resistant to oxidation and have been found to contribute to contaminant transport in rivers.[34] Finely dispersed metal sulfide colloids may resist aggregation and deposition, especially when stabilized by organic substances.[29] Improved knowledge of the mechanisms of colloidal particle formation under sulfate-reducing conditions and the factors promoting their stability in aqueous suspensions is therefore critical for developing conceptual models for the formation of colloids and their impact on the mobility of contaminants and nutrients.

Fe(III)-(oxyhydr)oxides, such as ferrihydrite (Fh ~$Fe(III)(OH)_3$), are redox-sensitive and ubiquitous in surface and near-surface environments. Under sulfate-reducing conditions, reductive dissolution of Fh can occur by electron transfer from dissolved sulfides produced by microbial sulfate reduction.[36-39] During the reaction of Fh with dissolved sulfide, oxidation of sulfide ions (to zero valent sulfur, S(0)) at mineral-water interfaces causes the release of dissolved Fe(II) into the aqueous phase.[40] The recent study by Kumar *et al.*[41] revealed that the ratio of dissolved sulfide to iron (sulfide/Fe) is a critical variable in the Fh sulfidation reaction. Reductive dissolution of Fh resulted in incremental releases of dissolved Fe(II) up to a sulfide/Fe ratio of 0.5, with Fe(II) concentrations declining sharply above this ratio, suggesting formation and settling of poorly crystalline iron monosulfide (FeS). However, dissolved Fe(II) is not thermodynamically stable in waters at circum-neutral pH values and should react with aqueous sulfide, resulting in the formation of aqueous FeS complexes as well as larger colloidal particles.[42] Aqueous FeS clusters, defined operationally in terms of their voltammetric characteristics, have been previously detected in natural (sub)surface water.[33,42,43] Thus, we posit that aqueous FeS clusters and/or larger colloidal particles are able

to resist aggregation that results in precipitation and can potentially sorb nutrients and contaminants and facilitate their transport under conditions outside of the solubility regime of the individual participating ions. Here, we found that the Fh sulfidation reaction generates FeS clusters and larger colloidal particles and determined the conditions required for their stability in aqueous suspensions.

Fh exhibits a high reactivity with natural organic carbon (NOC) and is often found either partially or completely covered by NOC in natural environments.[44-47] Thus, sulfidation reactions of Fh-organic composites could release NOC, which may affect the generation, nature, and stability of potential FeS colloids generated during sulfidation reactions of Fh, in addition to impacts on carbon export. The presence of organic ligands could inhibit the aggregation of aqueous FeS clusters into larger FeS colloidal particles, which was suggested by Rickard and Luther[42] but has not yet been demonstrated experimentally. In addition, organic ligands associated with FeS colloids could also cause these colloids to resist aggregation and deposition.[48] Consequently, the sulfidation of Fh-organic composites could modify the nature and stability of FeS colloids.

In order to better understand the conditions of formation, as well as the colloidal nature of FeS generated during sulfidation of Fh, our objectives in this study are to: (1) determine if Fh sulfidation as a function of sulfide/Fe ratio can result in the formation of FeS clusters and/or larger FeS colloids; (2) investigate the impact of NOC on the generation and stability of these FeS clusters and/or colloidal particles; and (3) develop a conceptual model for generation of stable FeS clusters and/or colloids, taking into account variabilities in groundwater composition, that can be used to predict colloidal behavior and impact on the sorption of metals, organic carbon, and nutrients by FeS colloids. The results of this study provide a framework of reaction rates and products dependent on the composition of the solid and aqueous fractions. Such information is important for determining if FeS colloid-facilitated transport should be incorporated into reactive transport models of groundwater.

2. MATERIAL AND ANALYTICAL PROCEDURE

2.1 Experimental Details

2.1.1 Ferrihydrite synthesis. Synthetic two-line ferrihydrite (Fh) was prepared by titrating 1 L of 104 mM aqueous solution of ferric chloride hexahydrate ($Fe(III)Cl_3 \cdot 6H_2O$) to a pH of 7.2-7.4 with 1M sodium hydroxide (300 mL).[49-50] The solution was first vigorously stirred while 200 mL of a 1M NaOH solution was added relatively quickly to bring the pH to 6.5; and the remaining 100mL of 1M sodium hydroxide was added drop wise for ~15 min until the pH reached 7.2–7.4. After hydrolysis, the precipitates were centrifuged (Spectrafuge 16M, Labnet International, USA) and the Fh nanoparticles were washed thoroughly (5-7 times) with Milli-Q water to remove salts, freeze-dried, and stored in an airtight amber glass tube at 4 °C until further use (no longer than 2 weeks). The degree of crystallinity and fraction purity of Fh were measured by X-ray diffraction analysis.[41] Total available surface area and particle sizes of the Fh prepared via this procedure have been previously reported as 332 m^2 g^{-1} and 5-7 nm, respectively.[41]

2.1.2 Organic compounds. Polyacrylic acid (PAA) and natural organic carbon (NOC) derived from plants were selected for this experiment to assess and contrast an organic molecule with a simple, single type of functional group (carboxylic functional groups in PAA[51]) *vs.* NOC, which contains a wider variety of functional groups representative of the complexity of organic matter in natural systems (NOC; Figure SI-1). The NOC in this case was composed of the water extractable organic carbon from 100g of grass freshly collected from a horse pasture (Riverton, WY). The grass was dried at 40°C for one week, cut into small pieces, and then extracted in 1 L Milli-Q water (in 1L glass bottle) on a continuous horizontal shaker (240 rpm) for 48 hours (h). The resulting aqueous fraction was filter-sterilized through 0.02 µm PES membrane filters (Millipore) to avoid the presence of bacteria. The chemical composition of NOC was analyzed by Fourier-Transform Ion Cyclotron Resonance Mass Spectrometry (FT-ICR-MS) as described in the supporting information (Figure SI-1).

2.1.3 Preparation of ferrihydrite-organic composites. A series of batch tests were performed using varying concentrations of PAA for a fixed mass of Fe(III)-(oxyhydr)oxides in order to determine the ideal concentration of PAA to optimize maximum sorption onto

Fe(III)-(oxyhydr)oxides surfaces (Figure SI-2). Thus a ratio of 200 mg C per g Fh was chosen for both PAA and NOC. To prepare the Fh-organic composites, 200 mg of washed and freeze-dried Fh was suspended in 20 mL MilliQ water containing 0.1M NaCl and stirred for 1h in order to achieve good homogeneity, and the pH was naturally around 6.8-7.0. The appropriate volumes of PAA or NOC were added to consistent aliquots of the Fh in suspension. The samples were reacted for 48h in the dark on a horizontal shaker table (240 rpm). Fh–PAA and Fh–NOC composites were centrifuged at 6000 rpm and dried at 35°C for 24h. Thereafter, the solids were transferred to the anoxic chamber (~4% H_2, 96% N_2) equipped with an O_2 detector and Pd catalyst (Coy Laboratories) and left open to equilibrate overnight. The Fh control (without any organic compounds) was also transferred to the anoxic chamber and allowed to equilibrate.

2.1.4 Sulfide solution. A stock solution of (0.5M) dissolved sulfide was prepared by dissolving sodium sulfide nonahydrate ($Na_2S{\bullet}9H_2O$) crystals (Acros, Belgium) in O_2-free Milli-Q water inside the anoxic chamber. The O_2-free water used throughout this study was prepared by bringing Milli-Q water to a boil and sparging with high purity N_2 gas while cooling down to room temperature (~ 4h).

2.2 Sulfidation reaction.

In this study, the variability of sulfide concentration added was measured against the Fe mass available to follow Fe-sulfide reaction (and product) at various stoichiometric ratios of Fe and dissolved sulfide. Focus of this study is to unravel the mechanistic of this reaction in controlled laboratory experiments and the role of sulfide/Fe stoichiometry in the process of colloid generation. The various stoichiometric ratios of Fe and dissolved sulfide chosen in this study stay however, representative of the variability of natural ecosystems between low magnitude typically observed in groundwater, wetland, and sediments[52], and marine and costal ecosystems[53].

A total of 200 mg of Fh nanoparticles was added to 65 mL of oxygen-free Milli-Q water (in 80 mL glass vials) containing 0.1M NaCl as a background electrolyte. The initial Fh nanoparticles are aggregated and settled into the 0.1M NaCl-solution immediately. Independent of the targeted sulfide/Fe ratio (sulfide/Fe =0.05; 0.1; 0.5; and 2.0), the same Fe concentration (*i.e.* the same mass of Fh) was used in all glass vials. Thereafter, an appropriate amount of sulfide solution was added to achieve the targeted sulfide/Fe ratio (*i.e.* 0.235,

0.470, 2.360, and 9.440 mL of 0.5M sulfide solution for ratios of 0.05, 0.1, 0.5, and 2, respectively). Vials were then closed with airtight rubber septa and aluminum crimp seals to restrict oxygen penetration and put on a continuous horizontal shaker (240 rpm). Aqueous and solid fraction samples were taken at different time intervals (3, 9, 24, 48, 120, 192 and 336h) after the addition of sulfide) inside the anoxic chamber using disposable needles and syringes. The retrieved samples were filtered through 0.02, 0.1, 0.22 and 0.45 µm PES filters (Millipore) using a filtration assembly that allows the preservation of the filter paper. Because no significant difference was observed in terms of total Fe concentration of the aqueous fraction passed through the different size filters, only the aqueous fraction that was filtered at 0.02 µm, *i.e.* 20 nm, is discussed in this paper. The aqueous fraction sample, defined as everything passing through 20 nm filters (Figure 1), was stored in 10 mL glass vials (closed with airtight septa) for further chemical analyses. The solid fraction, defined as everything retained on the 20 nm filter paper (Figure 1), was left to dry inside the anoxic chamber and kept air sealed in 10 mL glass vials until analysis with transmission electron microscopy.

The sulfidation reaction was repeated under exactly the same conditions for the Fh-PAA and Fh-NOC composites. The pH remained between 6.9 to 7.3 for all the sulfidation reactions tested (Table SI-1).

2.3 Chemical analysis of aqueous fraction.

Aqueous Fe(II) and Fe(III) were measured using a revised ferrozine method described by Viollier *et al.*[54] at a wavelength of 562 nm (limit of detection was 0.4µmol/L) using a Hewlett-Packard Vectra QS 165 spectrophotometer. Total Fe concentrations were determined by Inductively Coupled Plasma Optical Emission Spectrometry (ICP-OES). Certified reference materials and blanks were intercalated during the analytical series.

2.4 X-ray absorption spectroscopy (XAS) of aqueous fraction.

Fe *K*-edge X-ray Absorption Near Edge Structure (XANES) and Extended X-ray Absorption Fine Structure (EXAFS) spectra of the aqueous fraction filtered at 20 nm, were collected at 10 K (liquid He cryostat). Fluorescence-yield XANES and EXAFS spectra were collected using 30 or 100 pixel germanium detectors at beamline 7–3 and 9–3, respectively, at the Stanford Synchrotron Radiation Lightsource (SSRL). In order to avoid any oxidation, the preparation of samples was performed inside an anoxic chamber. The aqueous fraction was mixed with glycerol to avoid ice precipitation at 10 K (75% aqueous fraction: 25% glycerol),

then the mixture was loaded into a plastic holder with a Kapton® tape window, and finally the holder was mounted on the cryostat sample rod and brought to the beamline in a liquid nitrogen bath before being rapidly transferred into the liquid He cryostat. The Si(220) double crystal monochromator was detuned by 50% to minimize higher order harmonics and the beam energy was calibrated by setting the first *K*-edge inflection point of a Fe foil to 7112 eV (double transmission mode). A minimum of 7–16 spectra was collected for each sample to extract workable average spectra. No beam damage was detected. Fe *K*-edge spectra were averaged and normalized using the ATHENA software.[55] Fe *K*-edge EXAFS spectra were first analyzed by principal component analysis (PCA)[56] using the SIXPACK code[57] in order to estimate the minimum number of components necessary to fit these EXAFS spectra[58] (Tables SI-2). Finally, the species of Fe was determined by linear combination-least squares (LC-LS) fitting of the EXAFS spectra using the Athena program. The quality of the LC-LS fits was estimated by an R-factor parameter (R_f) of the following form: $R_f = (\chi_{exp} - \chi_{calc})^2 / (\chi_{exp})^2$. Shell-by-shell fitting was performed with the program ARTEMIS using the FEFF8 code 8.4.[59] Backscattering phase and amplitude functions were calculated using the FEFF8.4 program for Fe–S and Fe–Fe pairs. Fe–O pairs were also tested, but found not to be relevant.

2.5 Transmission electron microscopy (TEM) of solid fraction.

TEM images were acquired using a FEI Tecnai G2 F20 X-Twin (operating voltage of 200 kV) equipped with a field-emission gun, an X-ray detector (EDS) for compositional analysis, and a CCD camera; the point-to-point resolution was 2.5 Å. Dilute suspensions (prepared using O_2-free milliQ water) of the solid fraction (Figure 1) were deposited on ultra-thin holey carbon TEM grids and were dried under a nitrogen (97% N_2 + 3% H_2) atmosphere before TEM observations.

3. RESULTS

In this study, we define the aqueous fraction as everything passing through 20 nm filters, whereas that the solid fraction is defined as everything retained on the 20 nm filter paper (Figure 1). The size of nanoparticles of ferrihydrite and of his product of reduction, FeS, are lower than 20nm[41,42]. Consequently, we assume that the nanoparticles of ferrihydrite and FeS can be retain on the filter only if they form bigger aggregates, which are widely described to lead to the settling of these nanoparticles. In this manuscript, we exclude the aggregates as potential colloids as they can deposit, and we focus only on the Fe- and S-particles do not aggregate to in the ultimate goal to track on the particles remaining in suspension, *i.e.* colloids.

3.1 Correlation between aqueous fraction color and total Fe concentration.

We focus first on sulfidation of Fh in the absence of organic compounds. Immediate visual observation of the aqueous fractions separated using a 20 nm filter (Figure 1), collected after 3h of Fh sulfidation at different sulfide/Fe ratios, reveals a wide variation in color (Figure 2). The color intensity increased with increasing sulfide/Fe ratio, from light transparent green, for sulfide/Fe ratios of 0.05 and 0.1, to opaque black for sulfide/Fe ratios ≥ 0.5. The total Fe concentration increased in the aqueous fraction with increasing sulfide/Fe ratio (Figure 2). The quantity of Fe-containing species released into the aqueous fraction from Fh sulfidation is dependent on the sulfide/Fe ratio and the time since Fh sulfidation was induced, as discussed below.

Low sulfide concentration (sulfide/Fe ratio ≤0.5; Figure 2*).* During Fh sulfidation, the color of the freshly collected aqueous fraction (filtered at 20 nm) disappeared after 24h, 120h, and 192h after the start of Fh sulfidation for sulfide/Fe ratios of 0.05, 0.1, and 0.5, respectively. The total aqueous Fe concentration dropped from 2 mg/L (sulfide/Fe ratio = 0.05), 4 mg/L (sulfide/Fe ratio = 0.1), and 79 mg/L (sulfide/Fe ratio = 0.5) to below 1 mg/L concomitantly with the loss of color.

High sulfide concentration (sulfide/Fe ratio =2; Figure 2*).* The total Fe concentration in the aqueous fraction dropped significantly from 51 to 7 mg/L after 24h of Fh sulfidation and to 1 mg/L after 48h of Fh sulfidation. Concomitantly, the intensity of the color of the aqueous fraction decreased after 24h of Fh sulfidation, and after 48h no color was observed.

The sample colors and total aqueous Fe concentrations suggest that Fh sulfidation released colored Fe-containing phases during the first 24h (sulfide/Fe =0.05) to 192h (sulfide/Fe =0.5) after sulfidation was induced.

3.2 Residence time of colored Fe-containing aqueous phases.

The aqueous fractions filtered from Fh sulfidation reaction vials without organic compounds (separated using 20 nm filters) were allowed to settle for several days in order to observe the ability of colored Fe-containing phases to stay in suspension (Figure 1). The residence time of these phases in suspension is directly correlated with the sulfide/Fe ratio as described below.

Low sulfide concentration (sulfide/Fe ratio ≤0.5; Figure 2). Based on sample color, the Fe-containing phases generated from Fh sulfidation at a sulfide/Fe ratio of 0.1 are stable for several months if anoxic conditions are maintained. The total aqueous Fe concentration also remains stable for the same period of time. At a higher sulfide/Fe ratio of 0.5, the colored Fe-containing phases also remain stable in the aqueous fraction for a considerable, but shorter, period of time, ~14 days. After ~14 days, the Fe--containing phases aggregated, then settled. At that time, the total aqueous Fe concentration devoid of these aggregates (newly filtered using a 20 nm filter; Figure 1) dropped, which suggests that the colored Fe-containing phases are the main Fe-bearing constituent released during sulfidation of Fh or that these phases can sorb other dissolved Fe-containing phases.

High sulfide concentration (sulfide/Fe ratio >2; Figure 2). Based on color, Fe-containing phases aggregated, followed by settling in less than 24h, which resulted in a major, relatively rapid decline in aqueous Fe concentration.

Colored Fe-containing phases generated at sulfide/Fe ratios ≤0.5 remained in suspension for at least 14 days. The black coloration associated with these phases that aggregate and settle in time (for the sulfide/Fe ratio of 0.5) suggests that a significant fraction of these phases are colloidal. We will subsequently refer to these Fe-containing phases as FeS-colloids, and their chemical forms are detailed in §3.4.

3.3 Effect of organic compounds and ionic strength on Fe-containing aqueous phases.

Influence of organic compounds (Figure 3). Fh sulfidation experiments were carried out for two different types of Fh-organic composites: (i) polyacrylic acid (PAA) sorbed on the

surface of Fh, and (2) natural (water extractable) organic carbon (NOC) from grass sorbed on the surface of Fh. Overall, the presence of PAA or NOC sorbed on Fh before the addition of sulfide did not affect the visual appearance of the filtered aqueous fractions (20 nm) before settling. However, the maximum concentration of total Fe released into the aqueous fraction was systematically higher in the presence of organic compounds, especially with PAA, regardless of the sulfide/Fe ratio (Figure 3a). Moreover, the colored Fe-containing phase remained in the aqueous fraction longer in the presence of organic compounds than in Fh sulfidation experiments without organics (Figure 3b). Thus, the aqueous fractions (separated using 20 nm filters) collected immediately after inducing sulfidation of Fh-organic composites show that the color persists for more than 200h. In contrast, the color of the aqueous fraction collected during Fh sulfidation without sorbed organics disappeared after 120h at a sulfide/Fe ratio of 0.1 (Figure 3b).

Influence of ionic strength (Figure 4). Fh sulfidation initially performed with 0.1M NaCl as the background electrolyte, was also repeated with higher concentrations of NaCl in order to determine the effects of increased ionic strength of the aqueous fraction before the addition of sulfide. The total aqueous Fe concentration in the aqueous fractions with a concentration of NaCl above 0.15M dropped significantly (<1 ppm) only 3h after the Fh sulfidation reaction was induced (Figure 4). Concomitant with the drop in total aqueous Fe concentrations, the color of the aqueous fractions disappeared as well (Figure 4).

These observations show that the presence of organic compounds prolonged the time of formation and the quantity of Fe-containing phases, whereas an increase in ionic strength sped up the settling rate or inhibited colloid formation altogether.

3.4 Spectroscopic characterization of Fe-colloids.

FeS-colloids generated from Fh sulfidation at a sulfide/Fe ratio of 0.5 were quickly (within the day) analyzed by X-ray absorption spectroscopy in order to determine the number and types of Fe-containing species. In order to determine if the Fh sulfidation reaction time and the presence of organic compounds in the aqueous fraction had any effect on the molecular form of aqueous Fe, XAS analyses were performed on the filtered aqueous fractions (<20 nm) collected after 3h, 24h, 48h, and 120h of Fh sulfidation in the presence and absence of organic compounds (PAA or NOC; Figure 5). PCA indicates that 99% of the total variance of the system of all 12 EXAFS spectra collected for these Fe-colloids (<20 nm) can be explained by just one principal component (Table SI-2;[58]). Indeed, the similarity of Fe *K*-

edge XANES and EXAFS spectra of Fe-colloids in the absence and presence of organic compounds suggests that Fe is not complexed mainly with organic ligands (below 10% of the total Fe content, which is the detection limit;[60]). Furthermore, the similarity of Fe *K*-edge XAS spectra of Fe-containing colloids collected at different times after the Fh sulfidation reaction also suggests that aqueous Fe-containing colloids remained stable. However, a slight difference in the shape of the EXAFS spectra was systematically observed between Fe-containing colloids collected after 3h of Fh sulfidation and those collected after 24h, 48h, and 120h of Fh sulfidation (Figure 5), suggesting an evolution of two different Fe-containing species, as discussed below.

Low and rapid decrease of a ferrihydrite-colloidal phase. The intensity of oscillations is systematically lower for EXAFS spectra of the Fe-containing colloids collected after 3h of Fh sulfidation as compared to 24h, 48h, and 120h. The FT of the EXAFS spectrum of Fe-containing colloids collected after 3h of Fh sulfidation shows a feature centered at ~ 2.90 ± 0.1 Å (R+ΔR; Figure 5), which aligns well with Fe(III)−Fe(III) pair correlations characteristic of ferrihydrite (~ 2.97 Å (R+ΔR)). [41] The intensity of this feature decreases significantly between 3h and 24h of Fh sulfidation. This Fe(III)−Fe(III) pair correlation is not detectable after 48h or 120h of sulfidation. LC-LS fits of the Fe *K*-edge EXAFS spectra of Fe-containing colloids collected after 3h, using a Fh reference spectrum and the spectrum from Fe-containing colloids collected after 120h of Fh sulfidation, show that the Fh colloids represent, on average, 20% of the aqueous Fe after 3h of Fh sulfidation (Figure 6a and SI-4), independent of the presence or absence of organic compounds (Figure SI-4). However, addition of a Fh component in the fit of the EXAFS spectra from the 24h and 48h samples did not improved the fit quality.

In our experiments, the initial Fh nanoparticles were aggregated and settled before the addition of sulfide to the 0.1M NaCl-solution. Thus, the presence of a Fh colloid suggests that the sulfidation of Fh aggregates released Fh colloids at the beginning of the reaction and that this phase disappeared between 3h and 24h after sulfidation (Figure 6a). Fe(III) concentrations measured by colorimetry (revised ferrozine method) in the aqueous phase further corroborate this assumption that Fh colloids can be released during sulfidation of Fh aggregates (Figure SI-3). Moreover, Fe(III) is mainly detected in the aqueous fraction for sulfide/Fe ratios ≥0.5, suggesting that a minimum of sulfidation is required to mobilize Fh colloids (Figure SI-3). However, the exposure of mobilized Fh-colloids to dissolved sulfide could promote rapid reductive dissolution of this phase, which would explain the decreasing

amount of Fh-colloids after 3h of sulfidation. Additionally, He *et al.*[61] showed that zero-valent sulfur (S(0)) produced during Fh sulfidation can sorb on the surfaces of positively charged Fh nanoparticles, which should lead to extensive coagulation of Fh-colloids.

Mobilization of FeS colloids as aqueous FeS clusters. Despite the use of a large *k*-range (3-18 $Å^{-1}$), the FT of the EXAFS spectrum of the Fe-containing colloid collected after 120h of sulfidation shows only two major pair correlations; (i) a Fe(II)−S_1 pair at 2.24 Å (coordination number N fixed at 4) and (ii) a Fe(II)−$Fe(II)_1$ pair at 2.74 Å (N=1.8 ±0.3) identified by shell-by-shell fitting (Table SI-3). These two pair correlations are typical of FeS.[62] Minor frequencies (δR minimum resolvable distance = 0.08) of a second Fe(II)−S_2 pair correlation at 4.46 Å (N =2.3 ±1.2) and a second Fe(II)−$Fe(II)_2$ pair correlation at 3.84 Å (N =1 ±0.5) also improved the fit quality (Figure 6b). The number of Fe neighbors around the first shell of Fe ($N_{Fe\text{-}Fe1}$ =1.8 ±0.3), and the second shell of Fe ($N_{Fe\text{-}Fe2}$ =1 ±0.5) is lower than the value of 4 expected for an aggregated phase (nanoparticle), such as mackinawite.[63] Thus, the very low coordination numbers suggest the presence of a molecular form of FeS and not an FeS condensed phase. Luther *et al.*[35,64] proposed that during metal sulfide precipitation, the structure of the aqueous clusters is similar to that of the first condensed phase. The HR-TEM images of the settled solid fraction from our Fh sulfidation experiments clearly show the occurrence of structural layers with d-spacings characteristic of mackinawite (Figure 7). Our proposed structure is consistent with the molecular-level structure of the aqueous FeS clusters modeled by Luther and Rickard,[33] who suggested that the structure of smaller Fe_2S_2•$4H_2O$ clusters is similar to the basic layered structure of mackinawite. The shorter interatomic distances of the aqueous FeS clusters in our experiments compared to the structure of the smaller Fe_2S_2•$4H_2O$ and Fe_4S_4•$4H_2O$ clusters modeled by Luther and Rickard[33] suggest that our aqueous FeS clusters are more complicated intermediate phases with a slight contraction of the structure (Table 1). Furthermore, the Fe-Fe1 interatomic distances of aqueous FeS clusters in our experiments are longer than in the mackinawite structure and shorter than in the structure of smaller Fe_2S_2•$4H_2O$ clusters, which is consistent with the expected contraction of Fe-Fe distances in a larger FeS crystallite (Table 1). Fe–O pairs were also tested using shell-by-shell fitting, but were not found to improve the fit quality. We do not exclude the possible presence of dissolved Fe-hydroxy species or of hexaaquo Fe(II), but we consider these species to be at or below the detection limits of the fits of our EXAFS spectra (below 10% of the total Fe content, *i.e.* the detection limit;[60]), which corroborates the conclusion of Rickard and Luther.[42] Thus, the Fe-containing colloids generated during Fh

sulfidation, regardless of the presence or absence of organic compounds, are mainly FeS colloids.

3.5 TEM characterization of solid fraction.

HR-TEM was used to characterize the morphology of settled FeS nanoparticle aggregates from the solid fraction after 336h of Fh sulfidation. FeS nanoparticles are revealed by the presence of layered structures (d=5.5 Å; Figure 7). At a low sulfide/Fe ratio (= 0.5), we observed nanoparticles that do not exceed lengths of 5-8 nm; in addition, the layered structures have different orientations (Figure 7a). At a sulfide/Fe ratio of 2, we observed FeS nanoparticles that are significantly larger (31 nm in length) (Figure 7b), suggesting self-assembly into a nanoparticle with a crystallographically aligned layer structure.

4. DISCUSSION

4.1 Influence of sulfide/Fe ratios on the mobilization of FeS colloids.

Kumar *et al.*[41] proposed that reductive dissolution of Fh leads to the release of *dissolved Fe(II)* up to a sulfide/Fe ratio of ≤0.5 and the formation and settling of poorly crystalline FeS aggregates at sulfide/Fe ratios of >0.5. Results from the present study are consistent with the observation that dissolved Fe is removed from aqueous solution due to the settling of FeS aggregates at *high sulfide concentrations* (sulfide/Fe ratio >0.5). However, at *low sulfide concentrations* (sulfide/Fe ratio ≤0.5), our data reveal that Fe released to the aqueous fraction is mainly in the form of aqueous FeS clusters (Figure 6b). This result corroborates MINEQL+ modeling, which suggests that dissolved Fe(II) (hexaaquo Fe(II)) is of minor importance in sulfidic systems and becomes significant only at acidic pH values.[42] In addition to aqueous FeS clusters, we can not exclude the possible presence of other Fe-S complexes such as $FeSH^+$. However, in systems where Fe is more concentrated than sulfide (which is the case for sulfide/Fe ratios <0.5), Rickard and Luther[42] predicted that Fe-rich, polynuclear clusters should form, but not $FeSH^+$ (Figure 6; §3.4).

These results suggest that aqueous FeS clusters serve as precursors of larger FeS colloidal particles, which necessitates the following modification to the model proposed by Kumar *et al.*[41] for Fh sulfidation at low sulfide/Fe ratios. Fe(II) released from the reductive dissolution of Fh by dissolved sulfide produces *aqueous FeS clusters* at low sulfide/Fe ratios. As

observed in experiments from the present study, at *low sulfide concentrations* (sulfide/Fe ratio ≤0.5), aqueous FeS clusters resist aggregation for at least 14 days (Figure 2), behaving as FeS colloids. Conversely, at *high sulfide concentrations* (sulfide/Fe ratio >0.5), aqueous FeS clusters quickly aggregate and settle in less than 1 day. Thus, our new results indicate that the sulfide/Fe ratio has a major influence on mobilization of FeS colloids in low-temperature sulfidic environments, and subsequently on the mobilization of FeS colloids to which contaminants and nutrients sorb.

4.2 Stability of FeS colloids.

Kumar *et al.*[41] showed that Fh dissolution rates increase with increasing sulfide concentration up to a sulfide/Fe ratio of 0.5. In the present study we found an increase in the quantity of FeS colloids generated with increasing sulfide concentrations (Figure 8). Furthermore, the release of FeS colloids increased with the Fh sulfidation time according in a logarithmic relationships in our experiment, as shown for three different sulfide/Fe ratios in Figure 8. Once formed, the stability of FeS colloids in solution is also dependent on the sulfide/Fe ratio; the aggregation of FeS colloids increased up to a sulfide/Fe ratio of ≤0.5 (Figure 2). The direct correlation between the quantity of FeS colloids released into aqueous solution and the time before aggregation promotes their settling suggests that the sulfide/Fe ratio controls the mobility of FeS in the aqueous sulfide–iron system. Here, it is important to notify that the solubility of FeS in solutions above pH 6 is pH independent[42]. Thus, the mechanism of FeS precipitation from aqueous FeS is also not dependent on the pH, but mainly controlled by the sulfide/Fe ratio. However, the pH is a key parameter controlling the surface charge, which could directly impact the aggregation mechanisms.

Once released into aqueous solution, aqueous FeS clusters (0.5 to 2 nm[42]) can aggregate, leading to the formation of larger FeS nanoparticles (~2 nm[65]). These FeS nanoparticles can further aggregate and settle as an FeS solid phase (Figure 7). Based on Fe isotope studies, Wu *et al.*[66] proposed that the pH of the aqueous fraction drives the degree of FeS nanoparticle aggregation and, consequently, the degree of exchange between settled FeS nanoparticle aggregates (solid fraction) and aqueous FeS clusters (aqueous fraction). These authors proposed that at neutral pH, FeS nanoparticle aggregation is limited, which was more recently corroborated by morphologic studies.[67] This limited aggregation at neutral pH is due to the low isoelectric point of FeS[66] (~ pH 2), which results in strongly negative surface charges on FeS nanoparticles and electrostatic repulsion between nanoparticles at neutral pH. The pH_{PZC}

values for FeS were experimentally determined at 3.3 by Bebie *et al.*[68] and 2.9 by Widler and Seward[69]. Wolthers et al.[70] reported pH_{PZC} values of ~7.5 for FeS, however authors did state that the data reported could have been affected by oxidation, which is consistent for example with Dublet et al.[50], reporting pH_{PZC} values of ~7.9 for lab synthesized nanoparticulate 2-line ferrihydrite. In our experiments, the pH varied between 6.9 to 7.4, and increased systematically up to 0.4 pH values after 336h of Fh sulfidation for all sulfide/Fe ratios (Table SI-1). This increase of the pH could promote the aggregation of FeS nanoparticles generated from Fh sulfidation. Although, the increase of the pH is systematic for each sulfide/Fe ratio, while inversely, the stability of colloids over the time is changing drastically with the increase of sulfide/Fe ratio. So, even if FeS nanoparticle aggregation could potentially be triggered by increasing pH, the sulfide/Fe ratio remains the main factor controlling aggregation in our experiment.

The HR-TEM images of settled FeS nanoparticle aggregates suggest different crystallographic orientations of FeS nanoparticles depending on the sulfide/Fe ratio (Figure 7). The arrangement of FeS nanoparticles in aggregates generated at low sulfide/Fe ratio (sulfide/Fe ratio =0.5) was more chaotic than for FeS nanoparticles formed at high sulfide/Fe ratio (sulfide/Fe ratio =2) (Figure 7). Thus, we propose that the sulfide/Fe ratio, like pH, impacts the aggregation mechanism of the FeS nanoparticles and subsequently the stability of aqueous FeS clusters/colloids in aqueous solution, with aqueous FeS clusters/colloids being less stable with increased sulfide/Fe ratio. This hypothesis requires additional testing to determine the degree of aggregation and its impact on the mobilization of aqueous FeS clusters in the aqueous phase as a function of sulfide/Fe ratio, which could also contribute to colloid-facilitated transport of contaminants and nutrients.

4.3 Influence of organic compounds on the stability of FeS colloids.

The similarity of the chemical forms of Fe in FeS colloids in the absence and presence of organic compounds suggests that Fe-S complexation is more prevalent than Fe-organic complexation. Interaction of aqueous Fe(II) with the S ligands seems to be the key mechanism controlling Fe partitioning into the aqueous fraction. However, the presence of organic compounds prolonged the time of formation and the quantity of aqueous FeS colloids (Figure 3). The presence of organic molecules sorbed on Fh could retard Fh sulfidation, but this mechanism does not explain the systematic observation of higher concentrations of FeS colloids in the aqueous fraction in the presence of organic compounds than in their absence

(Figure 3). We thus hypothesize that the interaction of aqueous FeS clusters with organic compounds could increase the mobility of FeS colloids by retarding their aggregation into larger nanoparticles.

Organic compounds are known to influence the aggregation rates of nanoparticles by adsorbing the particles and inducing electrostatic and electrosteric repulsive forces that alter coagulation kinetics.[71-73] Few studies, however, have considered how organic compounds contribute to retarding aggregation.[42] Also, in spite of a number of studies, the stoichiometry of FeS clusters in the aqueous fraction is still unknown.[42] FeS cluster stoichiometries could include sulfur-rich varieties as well as Fe-rich species[34] and, more importantly, in natural systems these species will likely sorb a counter ion, such as organic molecules, to neutralize charge.[42] The possible sorption of organic ligands by aqueous FeS clusters and larger colloidal particles could induce repulsive forces between clusters and colloids. Such forces could explain the delay in aggregation and settling kinetics of FeS in the presence of organic compounds observed in our study in spite of the lack of change in the molecular structure of aqueous FeS clusters. It is well-known that organic substances contain metal-binding functional groups that influence precipitation kinetics by forming dissolved complexes with metals and lowering the mineral saturation index - the driving force for precipitation.[32,74,75] Similarly, organic ligands have been proposed to contribute to the stabilization and persistence of mobile zinc sulfide[75] and mercury sulfide[74,77] aqueous phases in aquatic environments.

Our results clearly show that the presence of the organic compounds we tested retards FeS colloid aggregation, but it does not inhibit aggregation. Nevertheless, the interaction of aqueous FeS clusters with organic compounds in natural systems could promote the formation of complexes with larger surface area and higher sorption capacity, potentially enhancing the adsorption of contaminants and nutrients.

4.4 Effect of solution ionic strength on mobilization of FeS colloids.

In addition to the previously discussed effects of sulfide/Fe ratios and the presence of organic compounds, our Fh sulfidation findings clearly show that the stability of FeS colloids is dependent on the ionic strength of the aqueous phase (Figure 4). Our results suggest that above an ionic strength of 0.15 M, mobilization of FeS colloids is inhibited. Indeed, the increase of ionic strength above 0.15 M NaCl dramatically accelerates aggregation, followed by settling of FeS nanoparticles in less than 3h (Figure 4). These observations suggest that

groundwater composition could play an important role in the mobilization of FeS colloids. In order to improve our ability to predict the types of environments more susceptible to mobilizing FeS colloids in groundwater, we used different types of artificial groundwater, characterized by different ionic strengths, to test the ability of Fh sulfidation to release FeS clusters and larger colloids that remain in suspension in the aqueous fraction for long periods of time. The focus of this study being to understand the impact of ionic strength observed in our experiment on release of FeS colloids in natural conditions, only groundwater characterized by neutral pH, pH of the experiment, were chosen, and any source of oxidants (nitrate and oxygen) were avoided The influence of the pH and oxidants will be deeply studied in a future study. The artificial groundwater were prepared to represent the following environments (Table SI-4): (1) Alpine river (*proxi of* alpine lake groundwater); Alluvial groundwaters with: (2) low ionic strength (Crested Butte groundwater, CO) and (3) high ionic strength (Riverton groundwater, WY); (4) Seawater (*proxi of* groundwater under marine influence) (Figure 9). These tests demonstrate that aqueous FeS cluster/colloid release and persistence in the aqueous fraction should mainly occur in low-salinity neutral pH groundwater systems where iron is enriched relatively to sulfide (1, and 2, at sulfide/Fe ratio ≤0.5); Figure 9). Thus, (sub)surface freshwaters poor in sulfate (*i.e.* characterized by low sulfidation), such as some fluvial or lacustrine systems, are the most susceptible to the mobilization of FeS colloids from Fh sulfidation. Importantly, this means that chalcophile contaminants and nutrients associated with FeS colloids in these environments would remain mobile under conditions outside of the solubility regime for the individual participating ions.

5. CONCLUSIONS AND ENVIRONMENTAL IMPLICATIONS

Our investigation provides a general conceptual model for predicting the release and stability of suspended FeS colloids. We show that sulfide/Fe ratio (≤0.5) as well as ionic strength (≤0.15M) are critical variables enabling mobilization of FeS colloids formed by sulfidation of ferrihydrite.

FeS colloids such as aqueous FeS clusters are responsible for basic electron transfer in many key biogeochemical pathways.[42] Thus, diffusion of FeS colloids could promote the electron shuttle influencing geochemical processes and microbial activities in groundwater aquifers. Our recent study[78] concluded that colloidal transport under reducing conditions could influence the spatial extent of biotic and abiotic sulfidic conditions in otherwise oxic aquifers. The interaction of FeS colloids with organic ligands in natural environments could also contribute to the mobilization of organic matter and nutrients in reducing environments.

Under anoxic conditions, FeS precipitation is widely known to transform and remove contaminants from groundwater, such as divalent metals,[79,80] chromium,[81] arsenic,[82-84] selenium,[85] uranium,[86,87] technetium,[88] tetrachloroethylene (PCE),[89] and halogenated organic compounds.[90] Our study indicates that in low-salinity fresh groundwater systems poor in sulfate (lakes, floodplains, peatlands *etc.*), the sulfidation reaction of ferrihydrite generates aqueous FeS clusters that remain suspended over long periods, thus mobilizing a substantial fraction of the total aqueous Fe and S. Luther and Rickard[33] proposed that these clusters could likely stabilize sulfide in oxic waters. Furthermore, these FeS colloids can directly bind nutrients and contaminants via sorption reactions and contribute to their transport in (sub)surface waters, which is corroborated by previous studies proposing that contaminant mobility in groundwater can be directly associated with FeS mobility in the aqueous fraction.[91] Our observations underline the potential effects of sulfate-reducing conditions, which can enable the transport of contaminants traditionally thought to be immobilized by FeS precipitation and settling. As a result, it is necessary for remediation assessments to include the possibility of FeS colloid-facilitated transport.

AKNOWLEDGMENTS

This research was supported by the DOE Office of Biological and Environmental Research, Climate and Environmental Sciences Division through the SLAC Groundwater Quality Science Focus Area program (Contract No. DE-AC02-76SF00515), by DOE-BES through its support of SSRL and by the DOE Office of Legacy Management. Financial support was also provided by the Center for Environmental Implications of NanoTechnology (CEINT), based at Duke University, through the U.S. National Science Foundation and the U.S. Environmental Protection Agency under NSF Cooperative Agreement EF-0830093/EF-1266252. SSRL and SLAC are supported by the U.S. DOE, under Contract No. DE-AC02-76SF00515, by the National Institutes of Health, National Institute of General Medical Sciences (including P41GM103393).

Matthew Latimer, Eric Nelson, and the technical staff at SSRL are gratefully acknowledged for their technical support during XAS measurements. The authors further thank Dr. Guangchao Li and Douglas Turner (Stanford University) for their great help in the ICP and TOC analyses, respectively.

REFERENCES

1. G. Heckrath, P.C. Brookes, P.R. Poulton and K.W.T. Goulding, Phosphorus leaching from soils containing different phosphorus concentrations in the Broadbalk experiment, *J. Environ. Qual.,* 1995, **24**, 904−910
2. L.W. De Jonge, P. Moldrup, G.H. Rubk, K. Schelde and J. Djurhuus, Particle leaching and particle-facilitated transport of phosphorus at field scale, *Vadose Zone J.,* 2004, **3**, 462−470
3. A. L. Vendelboe, P. Moldrup, G. Heckrath, Y. Jin and L.W. de Jonge, Colloid and phosphorus leaching from undisturbed soil cores samples along a natural clay gradient, *Soil Sci.* 2011, **176**, 399−406
4. D. Grolimund, M. Borkovec, K. Barmettler and H. Sticher, Colloid facilitated transport of strongly sorbing contaminants in natural porous media: A laboratory column study, *Environ. Sci. Technol.,* 1996, **30**, 3118−3123
5. A.D. Karathanasis, Subsurface migration of copper and zinc mediated by soil colloids, *Soil Sci. Soc. Am. J.,* 1999, **63**, 830−838
6. F.-A. Weber, A. Voegelin, R. Kaegi and R. Kretzschmar, Contaminant mobilization by metallic copper and metal sulphide colloids in flooded soil, *Nature Geosci,.* 2009*,* **2**, 267–271
7. B. Gao, Y. Dong, Y. Luo and L.Q. Ma, Colloid deposition and release in soils and their association with heavy metals, *Crit. Rev. Environ. Sci. Technol*., 2011, **41**, 336−372
8. J.E. Saiers and G.M. Hornberger, The role of colloidal kaolinite in the transport of cesium through laboratory sand columns, *Water Resour. Res.,* 1996, **32**, 33-41
9. M.I. Litaor, G. Barth, E.M. Zika, G. Litus, J. Moffitt and H. Daniels, The behavior of radionuclides in the soils of Rocky Flats, Colorado, *J. Environ. Radioact.,* 1998, **38**, 17−46
10. A.B. Kersting, D.W. Efurd, D.L. Finnegan, D.J. Rokop, D.K. Smith and J.L. Thompson, Migration of plutonium in groundwater at the Nevada Test Site, *Nature,* 1999, **397**, 56−59
11. A.P. Novikov, S.N. Kalmykow, S. Utsunomyia, R.C. Ewing, F. Horreard, A. Merkulov, S.B. Clark, V. Tkachev and B.F. Myasoedov, Colloid transport of plutonium in the far-field of the Mayak production association, *Russia. Science,* 2006, **314**, 638−641
12. T. Cheng and J.E. Saiers, Colloid-facilitated transport of cesium in vadose-zone sediments: the importance of flow transients, *Environ. Sci. Technol*., 2010, **44**, 7443−7449
13. Z. Liu, M. Flury, Z.F. Zhang, J.B. Harsh, G.W. Gee, C.E. Strickland and R.E. Clayton, Transport of europium colloids in vadose zone lysimeters at the semi-arid Hanford site, *Environ. Sci. Technol.,* 2013, **47**, 2153−2160
14. A.J.A. Vinten, B. Yaron and P.H. Nye, Vertical transport of pesticides into soil when adsorbed on suspended particles, *J. Agric. Food Chem*.,1983, **31**, 662−664
15. R. Lindqvist and C.G. Enfield, Biosorption of dichlorodiphenyltrichloroethane and hexachlorobenzene in groundwater and its implications for facilitated transport, *Appl. Environ. Microbiol.,* 1992, **58**, 2211−2218
16. L.A. Sprague, J.S. Herman, G.M. Hornberger and A.L. Mills, Atrazine adsorption and colloid-facilitated transport through the unsaturated zone, *J. Environ. Qual*., 2000, **29**, 1632−1641

17. B. Gjettermann, C.T. Petersen, C.B. Koch, N.H. Spliid, C. Grøn, D.L. Baun and M. Styczen, Particle-facilitated pesticide leaching from differently structured soil monoliths, *J. Environ. Qual.,* 2009, **38**, 2382−2392
18. T.A. Hanselman, D.A. Graetz and A.C. Wilkie, Manure-borne estrogens as potential environmental contaminants: A review, *Environ. Sci. Technol.,* 2003, **37**, 5471−5478
19. L.D. Steiner, V.J. Bidwell, H.J. Di, K.C. Cameron and G.L. Northcott, Transport and modeling of estrogenic hormones in a dairy farm effluent through undisturbed soil lysimeters, *Environ. Sci. Technol*., 2010, **44**, 2341−2347
20. Y. Zou and W. Zheng, Modeling manure colloid-facilitated transport of the weakly hydrophobic antibiotic florfenicol in saturated soil columns, *Environ. Sci. Technol.*, 2013, **47**, 5185−5192
21. J.F. McCarthy and J.M. Zachara, Subsurface transport of contaminant, *Environ. Sci. Technol.,* 1989, **23**, 496–502
22. R. Kretzschmar, M. Borkovec, D. Grolimund and M. Elimelech, Mobile subsurface colloids and their role in contaminant transport, *Adv. Agron.*, 1999, **66**, 121–193
23. A. Thompson, O.A. Chadwick, S. Boman and J. Chorover, Colloid mobilization during soil iron redox oscillations, *Environ. Sci. Technol*., 2006, **40**, 5743-5749
24. G.J. Lair, F. Zehetner, M. Fiebig, M.H. Gerzabek, C.A.M. Van Gestel, T. Hein, S. Hohensinner, P. Hsu, K.C. Jones, G. Jordan, A.A. Koelmans, A. Poot, D.M.E. Slijkerman, K.U. Totsche E. Bondar-Kunze and J.A. Barth, How do long-term development and periodical changes of river-floodplain systems affect the fate of contaminants? Results from European rivers, *Environ. Pollut,*. 2009, **157**, 3336–3346
25. J.M. Zachara, P.E., Long J.R. Bargar, J.A. Davis, P.M. Fox, J.K. Fredrickson, M.D. Freshley, A.E. Konopka, C. Liu, J.P. McKinley, M.L. Rockhold, K.H. Williams and S.B. Yabusaki, Persistence of uranium groundwater plumes: contrasting mechanisms at two DOE sites in the groundwater-river interaction zone, *J. Contam. Hydrol*., 2013,**147**, 45-72
26. S.F.L. Lynch, L.C. Batty and P. Byrne, Environmental risk of metal mining contaminated river bank sediment at redox-transitional zones, *Fortschr. Mineral*., 2014, **4**, 52–73
27. C. Schulz-Zunkel, J. Jörg Rinklebe and H.-R. Bork, Trace element release patterns from three floodplain soils under simulated oxidized–reduced cycles, *Ecol. Eng*., 2015, **83**, 485–495
28. S.B. Yabusaki, M.J. Wilkins, Y. Fang, K.H. Williams, B. Arora, J.R. Bargar, H.R. Beller, N.J. Bouskill, E.L. Brodie, J.N. Christensen, M.E. Conrad, R.E. Danczak, E. King, M.R. Soltanian, N.F. Spycher, C.I. Steefel, T.K. Tokunaga, R. Versteeg, S.R. Waichler and H.M. Wainwright, Water table dynamics and biogeochemical cycling in a shallow, variably-saturated floodplain *Environ. Sci. Technol.,* 2017, **51**, 3307-3310
29. L.M. Horzempa and G.R. Helz, Controls on the stability of sulfide soils: Colloidal covellite as an example, *Geochim. Cosmochim. Acta,* 1979, **43**, 1645–1650
30. C.H. Gammons and A.K. Frandsen, Fate and transport of metals in H_2S-rich waters at a treatment wetland, *Geochem. Trans.,* 2001, **2**, 1–15
31. J.W. Moreau, R.I., Webb and J.F. Banfield, Ultrastructure, aggregation-state, and crystal growth of biogenic nanocrystalline sphalerite and wurtzite, *Am. Mineral*., 2004, **89**, 950–960
32. B.L.T. Lau and H. Hsu-Kim, Precipitation and growth of zinc sulfide nanoparticles in the presence of thiol-containing natural organic ligands, *Environ. Sci. Technol*., 2008, **42**, 7236–7241

33. G.W. Luther III and D.T. Rickard, Metal sulfide cluster complexes and their biogeochemical importance in the environment, *J. Nanopart. Res*., 2005, **7** (4-5), 389-407
34. T.F. Rozan, M.E. Lassman, D.P. Ridge and G.W. Luther III, Evidence for iron, copper and zinc complexation as multinuclear sulphide clusters in oxic rivers, *Nature,* 2000, **406**, 879–882
35. G.W. Luther III, S.M. Theberge, T.F. Rozan, D. Rickard, C.C.,Rowlands and A. Oldroyd, Aqueous copper sulfide clusters as intermediates during copper sulfide formation, *Environ. Sci. Technol.,* 2002, **36**, 394–402
36. D.T. Rickard, Kinetics and mechanism of the sulfidation of goethite, *Am. J. Sci*., 1974, **274**, 941–952
37. A.J. Pyzik and S.E. Sommer, Sedimentary iron monosulfides: Kinetics and mechanism of formation, *Geochim. Cosmochim. Acta,* 1981, **45**, 687–698
38. D. Wei and K. Osseo-Asare, Aqueous synthesis of finely divided pyrite particles, *Colloids Surf. A,* 1997, **121**, 27–36
39. J.L. Druhan, C.I. Steefel, D. Molins, K.H. Williams, M.E. Conrad and D.J. DePaolo, Timing the onset of sulfate reduction over multiple subsurface acetate amendments by measurement and modeling of sulfur isotope fractionation, *Environ. Sci. Technol*., 2012, **46**, 8895–8902
40. R.A. Berner, Sedimentary pyrite formation: An update, *Geochim. Cosmochim. Acta,* 1984, **48**, 605–615
41. N. Kumar, J.S. Lezama-Pacheco, V. Noël, G. Dublet and G.E. Brown Jr., Sulfidation mechanisms of Fe(III)-(oxyhydr)oxide nanoparticles: A spectroscopic study, *Environ. Sci. Nano.,* 2018, **5**, 1012-1026
42. D.T. Rickard and G.W. Luther III, Chemistry of iron sulfides, *Chem. Rev*., 2007, **107** (2), 514–562
43. J. Buffle, R.R. de Vitre, D. Perret and G.G. Leppard, Combining field measurements for speciation in non perturbable waters, In *Metal Speciation: Theory, Analysis and Application*, Kramer, J.R., Allen, H.E., Eds., Lewis Publishers Inc. London, 1988, pp 99-124.
44. M.S. Torn, S.E. Trumbore, O.A. Chadwick, P.M. Vitousek and D.M. Hendricks, Mineral control of soil organic carbon storage and turnover, *Nature,* 1997, **389**, 170–173
45. K. Eusterhues, C. Rumpel and I. Kogel-Knabner, Organo-mineral associations in sandy acid forest soils: importance of specific surface area, iron oxides and micropores, *Eur. J. Soil Sci*., 2005, **56**, 753– 763
46. A.C. Cismasu, F.M. Michel, A.P. Tcaciuc, T. Tylisczcak and G.E. Brown Jr., Composition and structural aspects of naturally occurring ferrihydrite, *Comptes Rendus Geosci.,* 2011, **343**, 210-218
47. K. Lalonde, A. Mucci, A. Ouellet and Y. Gélinas, Preservation of organic matter in sediments promoted by iron, *Nature,* 2012, **483**, 198–200
48. S.W. Buettner, M.G. Kramer, O.A. Chadwick and A. Thompson, Mobilization of colloidal carbon during iron reduction in basaltic soils, *Geoderma*, 2014, **221–222**, 139-145
49. U. Schwertmann and R.M. Cornell, *Iron Oxides in the Laboratory: Preparation and Characterization*, 2nd edition, Wiley-VCH, Weinheim, Germany, 2003, 188 p.
50. G. Dublet, J.L. Pacheco, J.R. Bargar, S. Fendorf, N. Kumar, G.V. Lowry and G.E. Brown Jr., Partitioning of uranyl between ferrihydrite and humic substances at acidic and circum-neutral pH, *Geochim. Cosmochim. Acta,* 2017**, 215**, 122–140

51. N. Kumar, J. Labille, N. Bossa, M. Auffan, P. Doumenq, J. Rose and J-Y. Bottero, Enhanced transportability of zero valent iron nanoparticles in aquifer sediments: surface modifications, reactivity, and particle traveling distances, *Environ. Sci. Pollut. Res.,* 2017, **24**, 9269-9277
52. V. Noël, K. Boye, R.K. Kukkadapu, S. Bone, J.S. Lezama-Pacheco, E. Cardarelli, N. Janot, S. Fendorf, K.H. Williams, J.R. Bargar. (2017) Understanding controls on redox processes in floodplain sediments of the Upper Colorado River Basin. Science of the Total Environment. 603-604, 663-675.
53. V. Noël, C. Marchand, F. Juillot, G. Ona-Nguema, E. Viollier, G. Marakovic, L. Olivi, L. Delbes, F. Gelebart, G. Morin (2014) EXAFS analysis of iron cycling in mangrove sediments downstream a lateritized ultramafic watershed (Vavouto Bay, New Caledonia). Geochimica and Cosmochimica Acta. 136, 221-228.
54. E. Viollier, P.W. Inglett, K. Hunter, A.N. Roychoudhury and P. Van Cappellen, The ferrozine method revisited: Fe(II)/Fe(III) determination in natural waters, *Appl. Geochem*., 2000, **15**, 785–790
55. B. Ravel and M. Newville, ATHENA, ARTEMIS, HEPHAESTUS: data analysis for X-ray absorption spectroscopy using IFEFFIT, *J. Synchrotron Radiation,* 2005, **12**, 537–541
56. S.R. Wasserman, P.G. Allen, D.K. Shuh, J.J. Bucher and N.M. Edelstein, EXAFS and principal component analysis: a new shell game, *J. Synchrotron Radiation,* 1999, **6** (3), 284–286
57. S.M. Webb, SIXPack: A graphical user interface for XAS analysis using IFEFFIT, *Phys. Scripta,* 2005, **T115**, 1011–1014
58. E.R. Malinowski, Determination of the number of factors and the experimental error in a data matrix, *Anal. Chem*., 1977, **49** (4), 612–617
59. A.L. Ankudinov, B. Ravel, J.L. Rehr and S.D. Conradson, Real-space multiple-scattering calculation and interpretation of x-ray-absorption near-edge structure, *Phys. Rev. B: Condensed. Matter Mater. Phys.,* 1998, **58**, 7565-7576.
60. B. Cancès, F. Juillot, G. Morin, V. Laperche, L. Alvarez, O. Proux, G.E. Brown Jr. and G. Calas, XAS evidence of As(V) association with iron oxyhydroxides in a contaminated soil at a former arsenical pesticide processing plant, *Environ. Sci. Technol*., 2005, **39**, 9398–9405
61. L. He, L., Xie, D. Wang, W., Li, J.D. Fortner, Q. Li, Y. Duan, Z. Shi, P. Liao and C. Liu, Elucidating the role of sulfide on the sability of ferrihydrite colloids under anoxic conditions, *Environ. Sci. Technol.,* 2019, **53**, 4173−4184
62. A. Matamoros-Veloza, O. Cespedes, B.R.G. Johnson, T.M. Stawski, U. Terranova, N.H. de Leeuw and L.G. Benning, A highly reactive precursor in the iron sulfide system, *Nature Commun*., 2018, **9**, 3125.
63. A.R. Lennie, S.A.T. Redfern, P.F. Schofield and D.J. Vaughan, Synthesis and Rietveld crystal structure refinement of mackinawite, tetragonal FeS, *Mineral. Mag.*, 1995, **59**, 677–683
64. G.W. Luther III, S.M. Theberge and D.T. Rickard, Evidence for aqueous clusters as intermediates during zinc sulfide formation, *Geochim. Cosmochim. Acta,* 1999, **63**, 3159-3169
65. H. Ohfuji and D.T. Rickard, High resolution transmission electron microscopic study of synthetic nanocrystalline mackinawite, *Earth Planet. Sci. Lett.,* 2006, **241**, 227-233
66. L. Wu, G. Druschel, A. Findlay, B.L. Beard and C.M. Johnson, Experimental determination of iron isotope fractionations among Fe_{aq}^{2+} –FeS_{aq} –Mackinawite at low temperatures: Implications for the rock record, *Geochim. Cosmochim. Acta,* 2012, **89**, 46–61

67. A. Matamoros-Veloza, T.M. Stawski and L.G. Benning, Nanoparticle assembly leads to mackinawite formation, *Cryst. Growth Des.,* 2018, **18,** 6757−6764
68. J. Bebie, M.A.A. Schoonen, M. Furman and D.R. Strongin, Surface charge development on transition metal sulfides: an electrokinetic study, *Geochim. Cosmochim. Acta*, 1998, **62** (4), 633-642.
69. A.M. Widler and T.M. Seward, The adsorption of gold(I) hydrosulphide complexes by iron sulphide surfaces. Geochimica et Cosmochimica Acta, 2002, 66, 3, 1, 383-402.
70. M. Wolthers, L. Charlet, C.H. van Der Weijden, P.R. Van der Linde and D.T. Rickard, Arsenic mobility in the ambient sulfidic environment: sorption of arsenic (V) and arsenic (III) onto disordered mackinawite, *Geochim. Cosmochim. Acta,* 2005, **69** (14), 3483–3492
71. L. Liang and J.J. Morgan, Chemical aspects of iron-oxide coagulation in water - laboratory studies and implications for natural systems, *Aquat. Sci.,* 1990, **52** (1), 32–55
72. C.L. Tiller and C.R. O'Melia, Natural organic matter and colloidal stability: Models and measurements, *Colloids Surf. A,* 1993, **73**, 89–102
73. K.K. Au, A.C. Penisson, S.L. Yang and C.R. O'Melia, Natural organic matter at oxide/water interfaces: Complexation and conformation, *Geochim. Cosmochim. Acta,* 1999, **63** (19-20), 2903–2917
74. M. Ravichandran, G.R. Aiken, J.N. Ryan and M.M. Reddy, Inhibition of precipitation and aggregation of metacinnabar (mercuric sulfide) by dissolved organic matter isolated from the Florida Everglades, *Environ. Sci. Technol.,* 1999, **33** (9), 1418–1423
75. A.P. Gondikas, E.K. Jang and H. Hsu-Kim, Influence of amino acids cysteine and serine on aggregation kinetics of zinc and mercury sulfide colloids, *J. Colloid Interface Sci.*, 2010, **347** (2), 167–171
76. A. Deonarine, B.L.T. Lau, G.R. Aiken, J.N. Ryan and H. Hsu-Kim, Effects of humic substances on precipitation and aggregation of zinc sulfide nanoparticles, *Environ. Sci. Technol.,* 2011, **45**, 3217–3223
77. A. Deonarine and H. Hsu-Kim, Precipitation of mercuric sulfide nanoparticles in NOM-containing water: Implications for the natural environment, *Environ. Sci. Technol.,* 2009, **43** (7), 2368–2373
78. N. Kumar, V. Noël, B. Planer-Friedrich, J. Besold, J.S. Lezama-Pacheco, J. Bargar, G.E. Brown Jr., S. Fendorf and K. Boye, Heterogeneities promote thioarsenate formation and release into groundwater from low arsenic sediments, *Environ. Sci. Technol.,* Environ. Sci. Technol., 2020, 54, 3237−3244.
79. J.W. Morse and T. Arakaki, Adsorption and coprecipitation of divalent metals with mackinawite (FeS), *Geochim. Cosmochim. Acta,* 1993, **57** (15), 3635−3640
80. H.Y. Jeong, B. Klaue, J.D. Blum and K.F. Hayes, Sorption of mercuric ion by synthetic nanocrystalline mackinawite (FeS), *Environ. Sci. Technol.,* 2007, **41** (22), 7699−7705
81. R.R. Patterson, S. Fendorf and M. Fendorf, Reduction of hexavalent chromium by amorphous iron sulfide, *Environ. Sci. Technol.,* 1997, **31** (7), 2039−2044
82. T.J. Gallegos, S.P. Hyun and K.F. Hayes, Spectroscopic investigation of the uptake of arsenite from solution by synthetic mackinawite, *Environ. Sci. Technol.*, 2007, **41** (42), 7781−7786
83. H.Y. Jeong, Y.-S, Han, S.W. Park and K.F. Hayes, Aerobic oxidation of mackinawite (FeS) and its environmental implication for arsenic mobilization, *Geochim. Cosmochim. Acta,* 2010, **74** (11), 3182–3198

84. Y.S. Han, A.H. Demond, T.J. Gallegos and K.F. Hayes, Dependence of particle concentration effect on pH and redox for arsenic removal by FeS-coated sand under anoxic conditions, *Chemosphere,* 2015, **134**, 499–503
85. D.S. Han, B. Batchelor and A. Abdel-Wahab, Sorption of selenium (IV) and selenium (VI) to mackinawite (FeS): effect of contact time, extent of removal, sorption envelopes, *J. Hazard. Mater.,* 2011, **186** (1), 451–457
86. S.P. Hyun, J.A. Davis, K. Sun and K.F. Hayes, Uranium (VI) reduction by iron (II) monosulfide mackinawite, *Environ. Sci. Technol.,* 2012, **46** (6), 3369–3376
87. H. Veeramani, A.C. Scheinost, N. Monsegue, N.P. Qafoku, R. Kukkadapu, M. Newville, A. Lanzirotti, A. Pruden, M. Murayama and M.F. Hochella Jr., Abiotic reductive immobilization of U (VI) by biogenic mackinawite., *Environ. Sci. Technol*., 2013, **47** (5), 2361–2369
88. F.R. Livens, M.J. Jones, A.J. Hynes, J.M. Charnock, J.F.W. Mosselmans, C. Hennig, H. Steele, D. Collison, D.J. Vaughan, R.A.D. Pattrick, W.A. Reed and L.N. Moyes, X-ray absorption spectroscopy studies of reactions of technetium, uranium and neptunium with mackinawite, *J. Environ. Radioact.,* 2004, **74** (1−3), 211−219
89. D. Kyung, Y. Sihn, S. Kim, S. Bae, M.T. Amin, A.A. Alazba and W. Lee, Synergistic effect of nano-sized mackinawite with cyano-cobalamin in cement slurries for reductive dechlorination of tetrachloroethylene, *J. Hazard. Mater.,* 2016, **311**, 1–10
90. E.C. Butler and K.F. Hayes, Kinetics of the transformation of halogenated aliphatic compounds by iron sulfide, *Environ. Sci. Technol*., 2000, **34** (3), 422−429
91. N. Kumar, R-M. Couture, R. Millot, F. Battaglia-Bruner and J. Rose, Microbial sulfate reduction enhances arsenic mobility downstream of zerovalent iron based permeable reactive barrier, *Environ. Sci. Technol.*, 2016, **50**, 7610-7617.

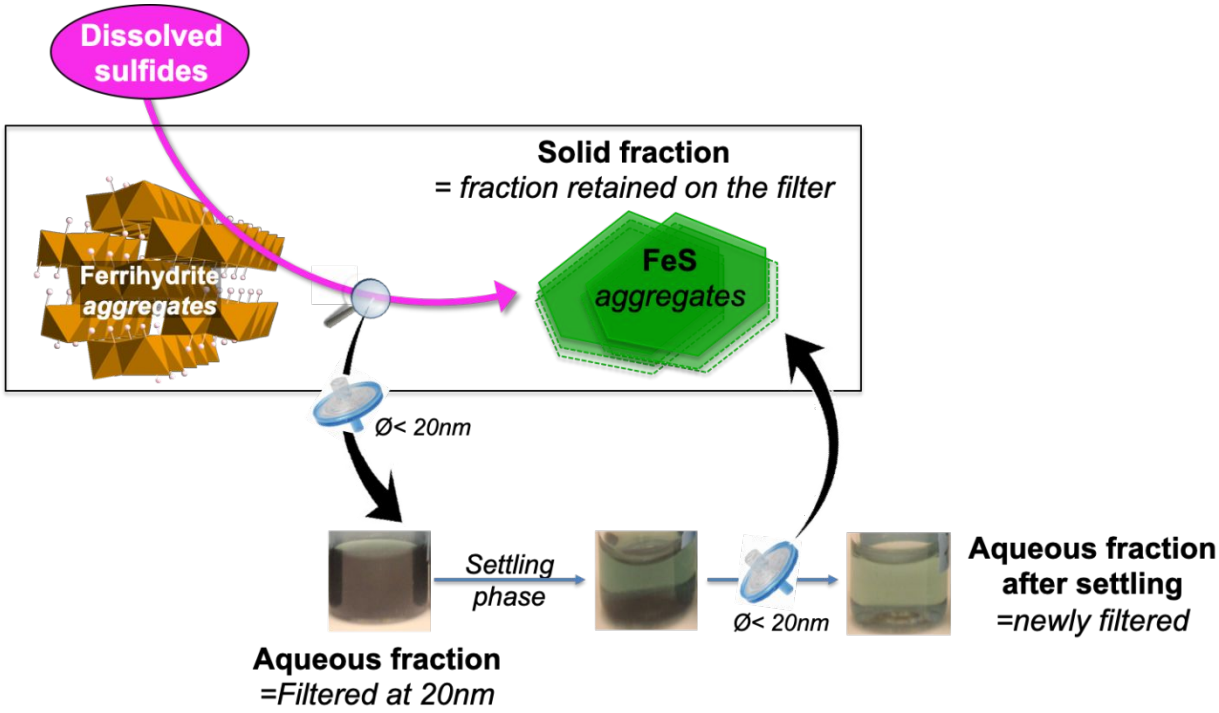

Figure 1. Schematics of the experimental approach and terminology used in this study to distinguish the solid fraction from the aqueous fraction (using a 20nm filter). The duration of settling of the solid fraction changed for each sulfide/Fe ratio as a function of the time needed for particles to condensate and/or aggregate as follows: 1, 14, and 50 days for sulfide/Fe ratios of 2, 0.5 and 0.1, respectively. After separation of the solid fraction, the aqueous fraction was filtered again using a 20nm filter in order to separate the newly formed solid fraction from that formed and aggregated during settling of the solid fraction. In all cases, the first filtration using a 20 nm filter was carried out immediately after sulfidation was initiated.

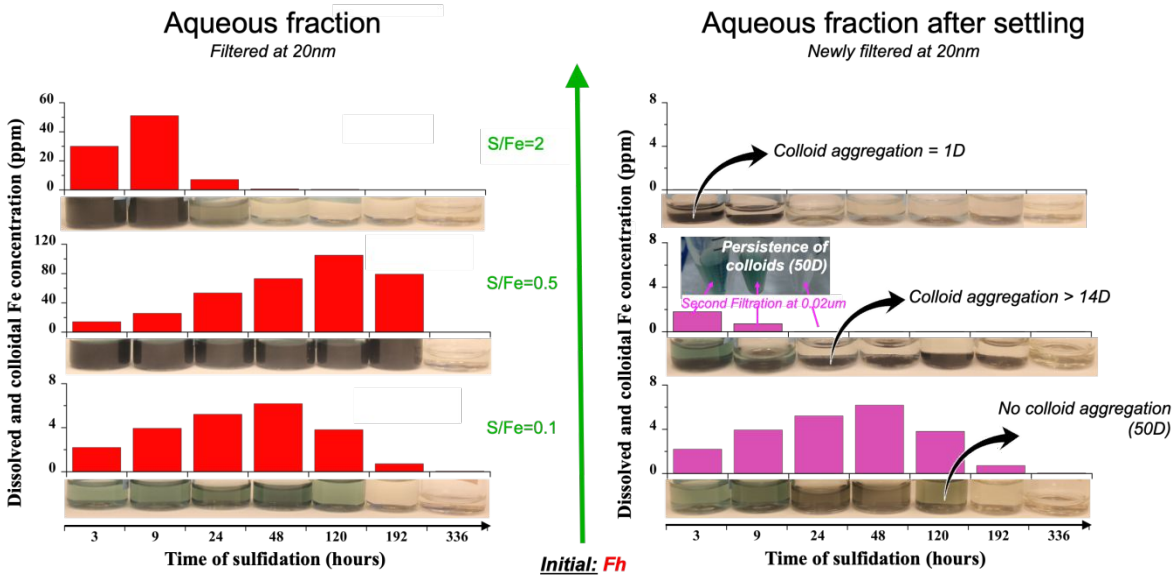

Figure 2. Left: Total Fe concentration and color intensity of the aqueous fraction (filtered using a <20 nm filter, before settling) from the reaction vials containing 0.1M NaCl-solution and a sulfide/Fe ratio of 0.1 (bottom), 0.5 (middle), and 2 (top) at 3, 9, 24, 48, 120, 192, and 336 hours (h) after the Fh (ferrihydrite) sulfidation reaction was initiated. **Right**: Coloration of the same aqueous fractions after the separation of a solid phase and total Fe concentration after a second filtration using a 20 nm filter.

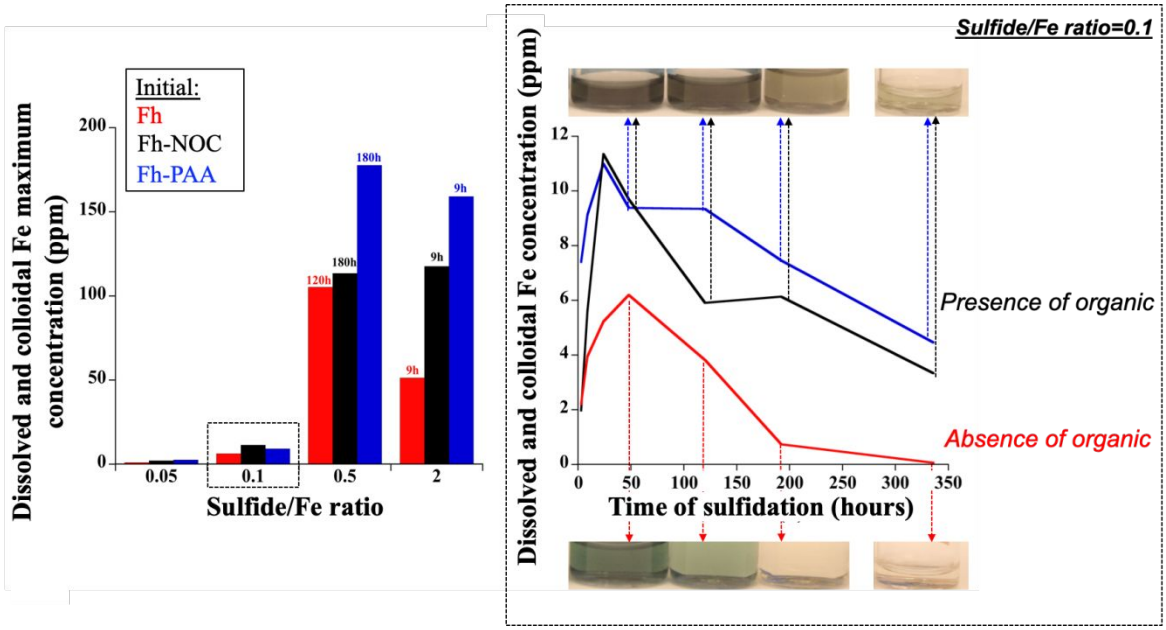

Figure 3. Left: Maximum total Fe concentration in the aqueous phase (<20 nm, before settling) during the sulfidation reaction of Fh (red), Fh-PAA (polyacrylic acid) composites (blue), and Fh-NOC (natural organic carbon, see §2.1.2) (black) composites, in a 0.1M NaCl-solution, as a function of sulfide/Fe ratios. **Right:** Evolution of total Fe concentrations and color intensity of the aqueous phase over time since initiation of sulfidation of Fh, Fh-PAA composites, and Fh-NOC composites in a 0.1M NaCl-solution for a sulfide/Fe ratio of 0.1.

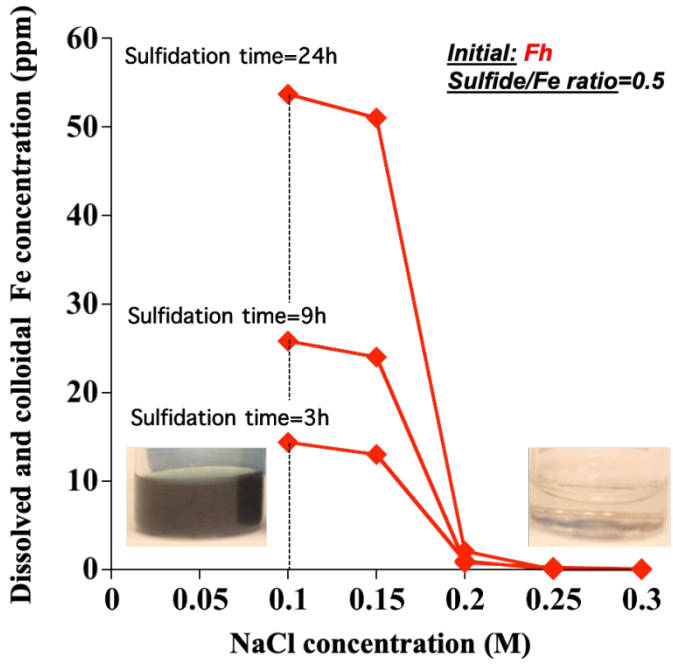

Figure 4. Total Fe concentration of the aqueous phase (<20 nm, before settling) as a function of molar concentrations of the background electrolyte, NaCl (as the background electrolyte). Concentrations were measured at 3, 9, and 24h after Fh sulfidation was initiated at a sulfide/Fe ratio of 0.1, which released significant quantities of colloids in the 0.1M NaCl-solution (dotted black line).

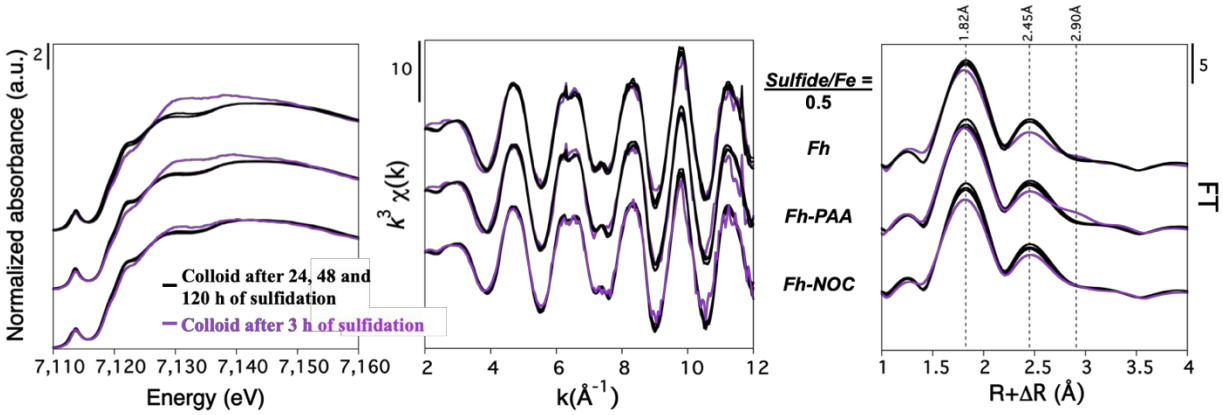

Figure 5. Fe *K*-edge (a) XANES spectra, (b) EXAFS spectra and (c) their Fourier transforms, of the aqueous fractions (<20 nm, before settling) collected from Fh sulfidation (top), Fh-PAA composites (middle), and Fh-NOC composites (bottom) in a 0.1M NaCl-solution, after 3h (in purple), and after 24, 48 and 120h (black) of reaction with dissolved sulfide at 0.5 sulfide/Fe ratio. Due to their spectral similarity, the EXAFS spectrum of the aqueous fractions collected after 24, 48 and 120h of sulfidation (in absence and presence of organic compounds) juxtaposes itself almost perfectly, which explain that we can't distinguish from each either on the figure.

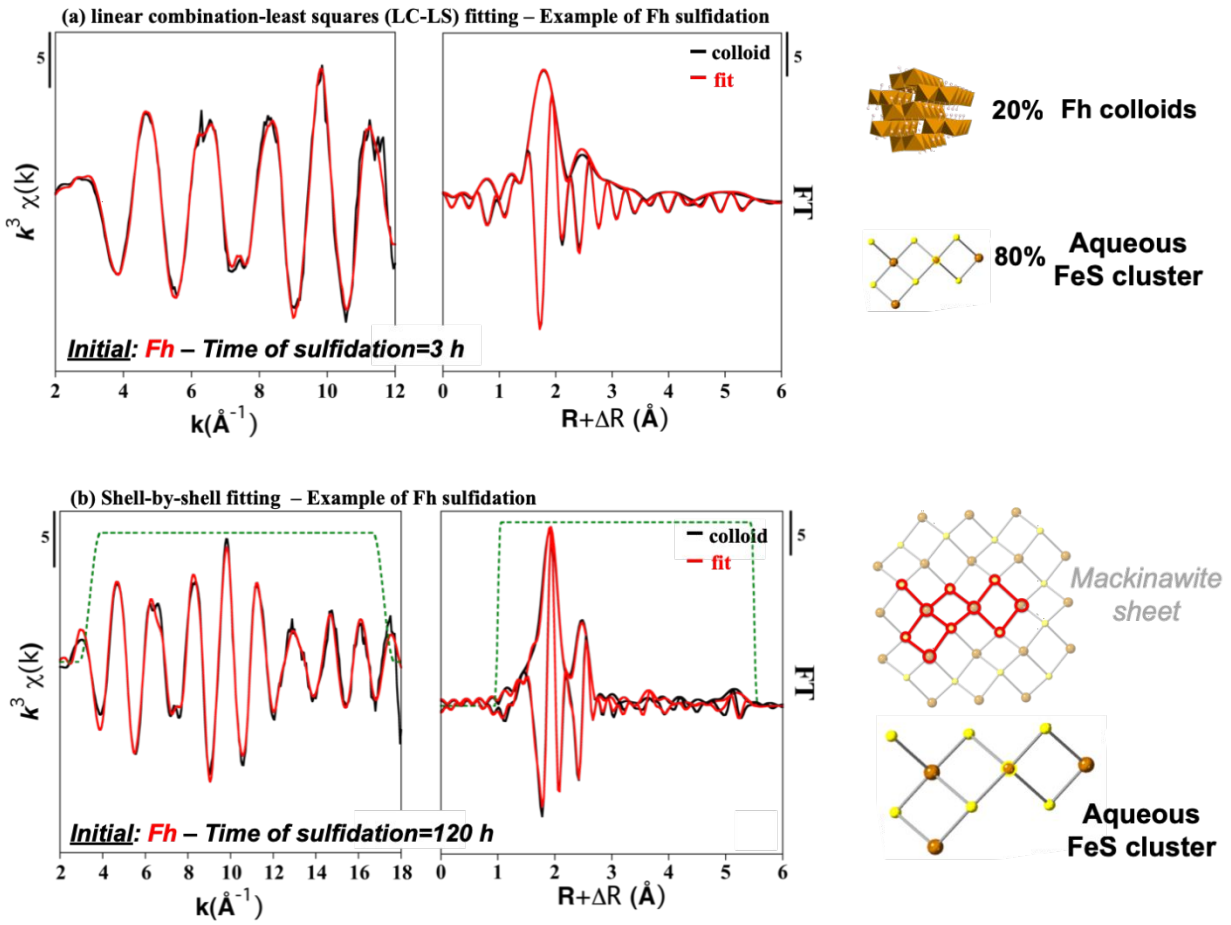

Figure 6. Molecular-level characterization of Fe in the aqueous fraction (<20 nm, before settling) from the sulfidation reaction of Fh at a sulfide/Fe ratio of 0.5 in a 0.1M NaCl-solution. (a) Linear combination-least squares fitting of the EXAFS spectrum of the aqueous fraction collected 3h after the Fh sulfidation reaction was initiated. The fitting was performed using a Fh reference spectrum and the spectrum from the aqueous fraction collected 120h after sulfidation reaction was initiated. (b) Shell-by-shell fits of EXAFS spectrum of the aqueous fraction collected 120h after Fh sulfidation reaction was initiated. The fitting range R = 1–5.5 Å and Fourier transform range: k = 3.4–16.8 $Å^{-1}$, are indicated by the green dotted line., homology between the structure of mackinawite and the aqueous FeS clusters identified as representing the colloids present in our samples (on the right).

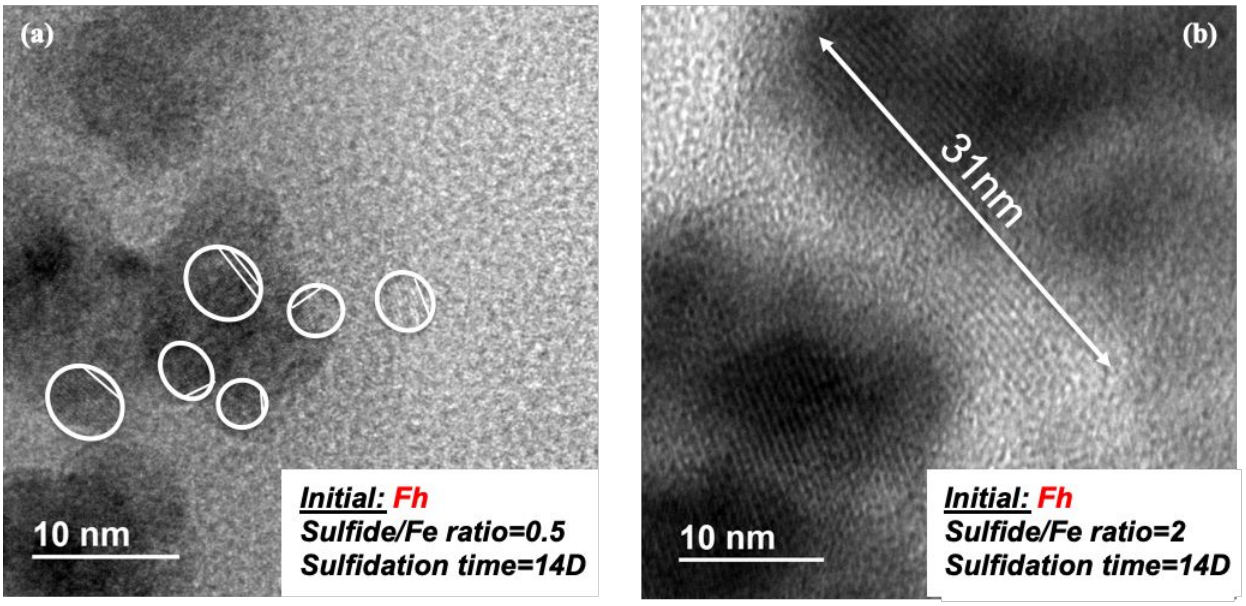

Figure 7. TEM images of the solid fraction (Figure 1) from sulfidation of Fh in a 0.1M NaCl-solution after 336h, for sulfide/Fe ratios of 0.5 (a) and 2 (b). The white circles and lines show the nanoparticles and the orientation of layers, respectively.

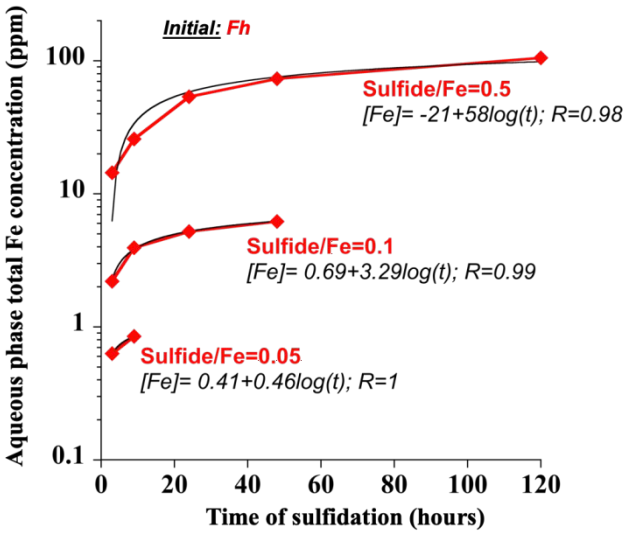

Figure 8. Total Fe concentration of the aqueous fraction (<20 nm, before settling) as a function of time since the sulfidation reaction was initiated in a 0.1M NaCl-solution for sulfide/Fe ratios of 0.05, 0.1, and 0.5 (red). The logarithmic functions describing the total Fe released in the aqueous fraction ([Fe]) as a function of the time of Fh sulfidation (t) are displayed for each sulfide/Fe ratio.

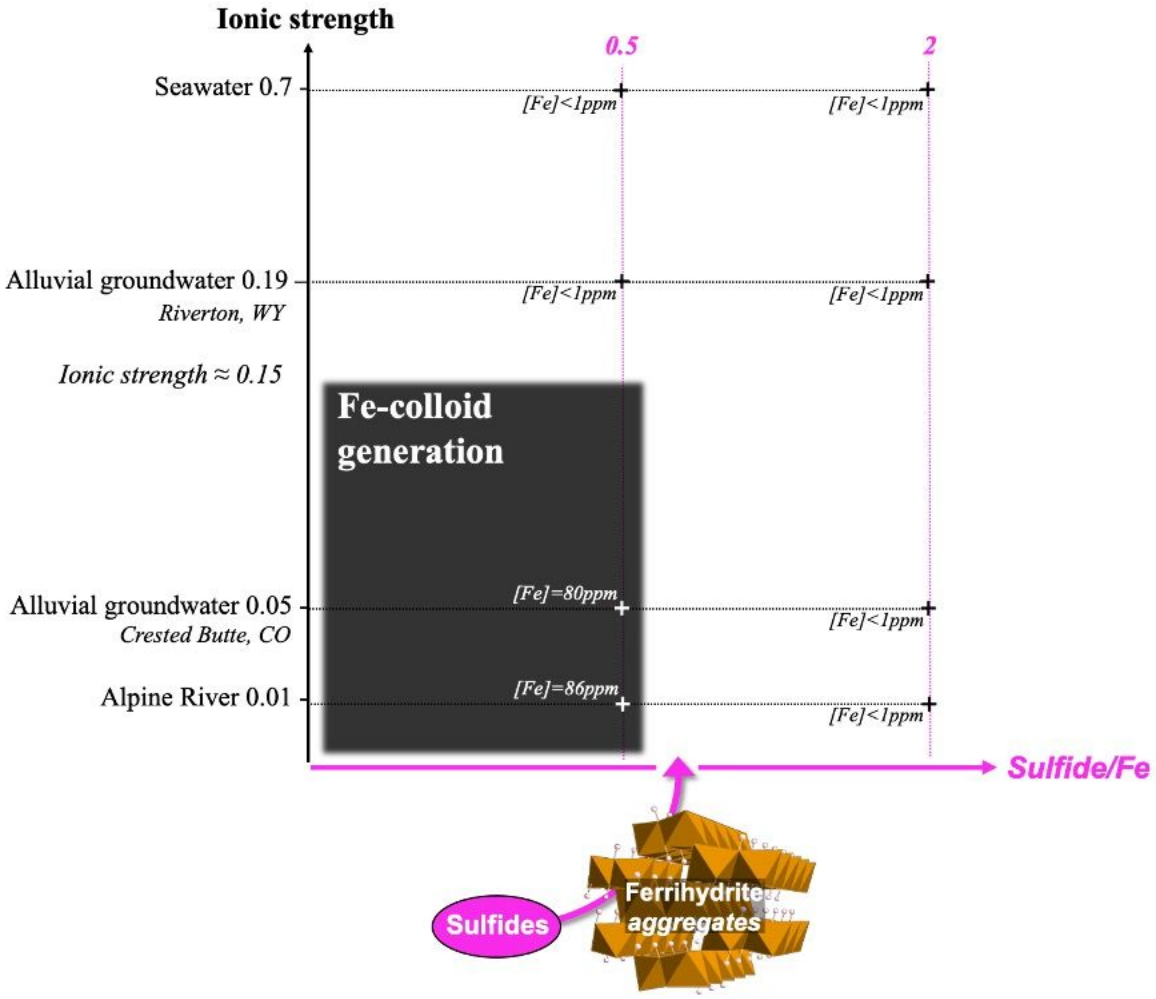

Figure 9. Total Fe concentration of aqueous fractions (<20 nm, before settling) collected 120h after the Fh sulfidation reaction for seven different types of groundwater for sulfide/Fe ratios (purple) of 0.5 and 2. The ionic strength was calculated from MinTeq, and the chemical compositions of each water sample are reported in Table SI. The black area represents the range of I.S. values and sulfide/Fe ratios required to generate FeS-colloids from Fh sulfidation.

Table 1. Homology between the structure of the simple aqueous FeS clusters, Fe_2S_2•$4H_2O$, and Fe_4S_4•$4H_2O$ calculated by Rickard et al. (2007) using the HYPERCHEM program, the aqueous FeS cluster resulting from Fh sulfidation collected after 120h (characterized in this study), and mackinawite in terms of interatomic distances. Dashes (-) indicate the absence of second-shell Fe-Fe and Fe-S.

	Fe_2S_2•$4H_2O$	**Fe_4S_4•$4H_2O$**	**FeS colloids from Fh sulfidation reaction (120h)**	**Mackinawite**
Fe–S1	2.201 Å	2.217 Å	2.238 Å	2.256 Å
Fe–Fe1	2.833 Å	2.800 Å	2.741 Å	2.560 Å
Fe–Fe2	-	-	3.839 Å	3.670 Å
Fe–S2	-	-	4.450 Å	4.310 Å